Fermi National Accelerator Laboratory

FERMILAB-Pub-86/83-A
May 1986

Kinematic Tests of Exotic Flat Cosmological Models

Jane C. Charlton[a] and Michael S. Turner[a,b,c]

[a]Astronomy and Astrophysics Center
The University of Chicago

[b]Department of Physics and the Enrico Fermi Institute
The University of Chicago

[c]NASA/Fermilab Astrophysics Center
Fermi National Accelerator Laboratory

Abstract

Theoretical prejudice and inflationary models of the very early Universe strongly favor the flat, Einstein-deSitter model of the Universe. At present the observational data conflict with this prejudice. This conflict can be resolved by considering flat models of the Universe which possess a smooth component of energy density. We study in detail the kinematics of such models, where the smooth component is relativistic particles, a cosmological term, a network of light strings, or fast-moving, light strings. We also discuss the observational tests which can be used to discriminate between these models. These tests include the magnitude-redshift, lookback time-redshift, angular size-redshift, and comoving volume-redshift diagrams and the growth of density fluctuations.

Operated by Universities Research Association Inc. under contract with the United States Department of Energy

I. Introduction

One of the most fundamental questions we can ask about the Universe is, how much matter is there in it? Luminous matter contributes but a small fraction of the critical density: $\Omega_{LUM} \simeq 0.01$ (see, e.g., Faber and Gallagher 1979). The flat rotation curves of galaxies (Rubin, Ford, and Thonnard 1978,1980; Bosma 1981a,b; Rubin 1983) and the virial mass determinations of clusters of galaxies (Faber and Gallagher 1979) indicate that the dominant component of the mass density in the Universe is dark and that the dark component is ubiquitous and contributes $\Omega_{DARK} \gtrsim 0.1$. The total amount of dark matter and its composition are at present still unknown. (For a recent review of dark matter in the Universe, see Kormendy and Knapp 1986.) Primordial nucleosynthesis constrains the fraction of critical density contributed by baryons to be $\Omega_b \lesssim 0.35h^{-2}$ (Yang etal. 1984) where as usual the present value of the Hubble parameter is written as, $H_0 = 100\ h\ km\ s^{-1} Mpc^{-1}$. It follows that if $\Omega_{TOT} \gtrsim 0.2$, then the dark component must be non-baryonic. Modern particle physics theories have provided an ample list of candidate particles whose relic abundances would allow them to account for the dark matter (for a recent discussion, see, Turner 1986).

Essentially all measurements of the amount of matter that clusters on scales $\lesssim$ 10–30Mpc strongly suggest that $\Omega_{10-30} \simeq 0.1$–$0.3$ (see, e.g., Faber and Gallagher 1979; Press and Davis 1982; Audouze and Tran Thanh Van 1983; Davis and Peebles 1983). We must emphasize that such measurements are insensitive to a component(s) which is smoothly distributed on these scales. While in principle the deceleration parameter is sensitive to the total amount of matter in the Universe (smooth and clumped), attempts to determine it unambiguously have thus far been unsuccessful (see, e.g., Gunn and Oke 1975; Kristian, Sandage, and Westphal 1978; Huchra 1986; Sandage and Tammann 1986). It goes without saying that the amount, nature, and distribution of dark matter in the Universe are

among the most pressing questions facing cosmologists today.

Theory is not without its opinions. Because of the inherent instability of an $\Omega \neq 1$ Universe (Dicke and Peebles 1979) theoretical prejudice strongly favors the flat, Einstein-deSitter model ($\Omega = 1$). Indeed, the inflationary Universe scenario proposed by Guth (1981) (and modified by Linde 1982 and Albrecht and Steinhardt 1982) provides the means of guaranteeing that the Universe is very flat today, regardless of its initial curvature.

If, as theoretical prejudice favors, the Universe is flat, then cosmologists are faced with a dilemma: either the measurements of the amount of matter which clumps on scales $\lesssim$ 10–30Mpc are wrong, or they are misleading, as they suggest that $\Omega \simeq 0.1$–0.3. Theoretical prejudice and cosmological observations can be reconciled if the bulk of the matter in the Universe ($\Omega_{SM} = 1 - \Omega_{10-30} \simeq 0.7$–$0.9$) resides in a component that is smoothly distributed on scales $\lesssim$ 10–30Mpc. A number of possibilities, motivated by early Universe physics, have been suggested for the hypothetical smooth component. They include: (i) Relativistic or very fast-moving ($v \gtrsim 10^{-2}\ c$) particles produced by the recent decay of unstable, relic particles, which, by virtue of their high speeds, cannot clump (Dicus, Kolb, and Teplitz 1977; Turner, Steigman, and Krauss 1984; Gelmini, Schramm, and Vallee 1984; Olive, Seckel, and Vishniac 1985); (ii) A relic cosmological term (which corresponds to a uniform energy density throughout the Universe) (Peebles 1984; Turner, Steigman, and Krauss 1984); (iii) A network of light strings, or very fast-moving light strings (Vilenkin 1984). (These light strings are not to be confused with the more familiar heavy cosmic strings which can induce significant density perturbations in the matter. For a recent review of cosmic strings, both heavy and light, see Vilenkin (1985).) ; (iv) Failed galaxies, by which one means galaxies that, because of their faintness, have not been detected, and are more smoothly-distributed than bright galaxies (Kaiser 1986; Bardeen, Bond, Kaiser,

and Szalay 1986).

For possibilities (i-iii) the bulk of the mass density in the Universe would reside in a component whose density does not decrease like that of non-relativistic matter (i.e., different from $\rho \propto a^{-3}$, where a = the Robertson-Walker cosmic scale factor). Therefore, the kinematics of these models will be very different from those of the conventional matter-dominated, Einstein-deSitter model. These differences could, in principle, be exploited to discriminate between (and hopefully rule out) some of the myriad of models.

The purpose of our paper is to explore this possibility. We calculate the evolution of the cosmic scale factor in these exotic Einstein-deSitter models and consider the classical cosmological tests (magnitude-redshift, angle-redshift, look-back time-redshift, and comoving volume-redshift diagrams), as well as growth of density perturbations in the clumped component. Of course there are other observational probes we have not considered here. Among them are the predicted anisotropies in the cosmic microwave background (see, e.g., Turner 1985a; Vittorio and Silk 1985; Kolb, Olive, and Vittorio 1986), and the predicted large-scale peculiar velocity fields (Kaiser 1983; Vittorio and Silk 1985; Vittorio and Turner 1986), which result from the primordial density perturbations necessary for structure formation.

II. Notation and the Models

The evolution of the scale factor, a, in a Friedmann-Robertson-Walker cosmology is governed by the Friedmann equation,

$$H^2 = \left(\frac{\dot{a}}{a}\right)^2 = \frac{8\pi G}{3}\rho + \frac{\Lambda}{3} - \frac{k}{a^2}, \tag{1}$$

where ρ is the total energy density, k/a^2 is the curvature contribution, and Λ is the cosmological term. For the most general case ρ is given by a sum of all possi-

ble contributions:

$$\rho=\rho_{NR}+\rho_R+\rho_{FS}+\rho_{NET}+\rho_X+\rho_{RX}, \tag{2}$$

where NR represents stable non-relativistic particles which can clump; R, relativistic particles; FS, light, fast-moving, non-intercommuting strings; NET, a network of light strings; X, a decaying massive, NR particle species; and RX, the relativistic particles produced by X decays. Throughout we will specify the contribution of each term to the right hand side of equation (1) by its fraction of the critical density ($\rho_{crit}=3H_0^2/8\pi G \simeq 1.88h^2\times10^{-29}gcm^{-3}$):

$$\Omega_i=\frac{8\pi G\rho_i}{3H_0^2} \qquad i=NR,R,RX,X,FS,NET \tag{3a}$$

$$\Omega_\Lambda=\frac{\Lambda}{3H_0^2}, \tag{3b}$$

$$\Omega_k=\frac{-k}{H_0^2a_0^2}, \tag{3c}$$

By definition $\sum_i\Omega_i=1$. Omitting, for now, the possibility of decaying particles, the Friedmann equation can be rewritten:

$$H^2=\left(\frac{\dot a}{a}\right)^2=H_0^2\left[\Omega_{NR}\left(\frac{a}{a_0}\right)^{-3}+\Omega_R\left(\frac{a}{a_0}\right)^{-4}+\Omega_{FS}\left(\frac{at}{a_0t_0}\right)^{-1}+\Omega_\Lambda\right.$$
$$\left.+\Omega_{NET}\left(\frac{a}{a_0}\right)^{-2}+\Omega_k\left(\frac{a}{a_0}\right)^{-2}\right]. \tag{4}$$

where subscript 'o' denotes the present epoch.

The component in non-relativistic particles deserves further comment. Its mass density varies as a^{-3}, not only for normal baryonic material but also for the more exotic cold and hot dark matter candidates which are non-relativistic today. For our purposes all NR particles which can undergo clustering are lumped into Ω_{NR}. It is this component to which the observations are sensitive, and determine to be $\Omega_{NR}\simeq\Omega_{10\text{-}30}\simeq 0.2\pm0.1$.

Rather than considering the most general model we will consider two component models with NR particles and a smooth component. As two simple

limiting models we will consider the cases $\Omega_{NR}=1$, where

$$\frac{H}{H_0}=\left(\frac{a}{a_0}\right)^{-3/2}, \tag{5a}$$

and $\Omega_R=1$, for which

$$\frac{H}{H_0}=\left(\frac{a}{a_0}\right)^{-2}. \tag{5b}$$

The latter model for many purposes is a very simple approximation to the more realistic case where the relativistic particles are produced by decaying relics. For the remaining models we choose Ω_{NR} in the range 0.1-0.3 and a smooth component with $\Omega_{SM}=1-\Omega_{NR}$. If this smooth component is a relic cosmological term (Peebles 1984; Turner, Steigman, and Krauss 1984)

$$\Omega_\Lambda=1-\Omega_{NR}=\frac{\Lambda}{3H_0^2}, \tag{6}$$

and equation (4) simplifies to

$$\frac{H}{H_0}=\left[\Omega_\Lambda+\Omega_{NR}\left(\frac{a}{a_0}\right)^{-3}\right]^{1/2}. \tag{7}$$

For fast-moving strings, $\rho_{FS}\,\alpha\,1/(t\,a(t))$ and so if the smooth component is fast-moving cosmic strings (Vilenkin 1984; also see Turner 1985b), the evolution of the scale factor is governed by

$$\frac{H}{H_0}=\frac{\dot{a}}{a}=\left[\Omega_{NR}\left(\frac{a}{a_0}\right)^{-3}+\Omega_{FS}\left(\frac{at}{a_0t_0}\right)^{-2}\right]^{1/2}. \tag{8}$$

The solution of equation (8) is discussed in the Appendix.

A third possibility for the smooth component is relativistic particles produced by the decay of an unstable massive relic particle species, X. This case is discussed in detail by Turner (1985c). We will not repeat his calculations here but will simply present his results and compare them to the other models. Following Turner (1985c) we define the ratio of the mass density in unstable particles (before decay) to that in the stable NR component to be $\beta^{-1}=\rho_X/\rho_{NR}$. β^{-1} is

related to the redshift of decay $(1+z_D)$, Ω_{NR}, and Ω_R by $\beta^{-1}=(\Omega_R/\Omega_{NR})(1+z_D)$. The small scale isotropy of the microwave background restricts $1+z_D$ to be less than or of order 10 (Turner 1985a; Vittorio and Silk 1985; Kolb, Olive, and Vittorio 1986) and with $\Omega_{NR}=0.2\pm0.1$, $\Omega_R/\Omega_{NR}=2.3$–9, so that the range of interest for β^{-1} is 3–100.

Finally, for purposes of comparison, we will consider non-flat models ($k<0$). For these models equation (4) reduces to

$$\frac{H}{H_0}=\left[\Omega_{NR}\left(\frac{a}{a_0}\right)^{-3}+\Omega_k\left(\frac{a}{a_0}\right)^{-2}\right]^{1/2}. \tag{9}$$

Since $\rho_{NET}\propto a^{-2}$, this equation (with Ω_k replaced by Ω_{NET}) also describes models in which the smooth component is a string network. Equations (5a), (5b), (7), (8), (9) and a similar equation for the decaying particle model can be solved to yield the evolution of the scale factor, $a(t)$, for each model. All of the kinematic discriminators we shall discuss depend solely upon the evolution of $a(t)$, and so we show the evolution of the scale factor, $a(t)$, in Figure 1, for the various models.

The scale factor may be expressed as a power series expanded about the present epoch (see, e.g., Weinberg 1972):

$$a(t)=a(t_0)\left[1+H_0(t-t_0)-\frac{1}{2}q_0H_0^2(t-t_0)^2+\cdots\right] \tag{10}$$

where the deceleration parameter $q_0\equiv-\ddot{R}(t_0)R(t_0)/\dot{R}^2(t_0)$. Using the Einstein equations, this parameter can be written as

$$q_0=\frac{1}{2}(1+3\Omega_{SM}\gamma_{SM}) \tag{11}$$

where $\gamma_{SM}\equiv p_{SM}/\rho_{SM}|_{t_0}$ is the ratio of the pressure in the smooth component to the energy density in the smooth component and has the values:

$$\gamma_{SM}=\begin{cases}-1 & \Lambda\neq0\\ -1/3 & k<0,\ FS,\ NET\\ 0 & NR\\ 1/3 & R\end{cases} \tag{12}$$

The parameter q_0 serves to parameterize the recent behavior of the scale factor. Most of the kinematical differences between the models can be qualitatively understood in terms of the relative pressure in the smooth component (i.e., γ_{SM}).

III. Kinematics

In sections (IIIa) - (IIIg), possible observational means of distinguishing between cosmological models will be considered. Unfortunately none of the observations have yet been refined to the extent that we can make definitive statements concerning the viability of any of the models. However, with the advent of the Space Telescope, a new generation of large, ground-based telescopes, and other new instruments (such as SIRTF), many of the observations, on which the various discriminators depend, may be made in the foreseeable future. Throughout this section we assume that the reader is familiar with the basic kinematics of the Friedmann-Robertson-Walker models. For more details and the derivation of the standard results we refer the reader to Weinberg (1972) or another similar text on cosmology.

A. Age-redshift diagram

The general expression for the age of the Universe is:

$$t = \int_0^{a(t)} da/\dot{a} \tag{13a}$$

$$H_0 t = \int_0^{(1+z)^{-1}a_0} da/\left[a(H/H_0)\right]. \tag{13b}$$

This integral can be evaluated analytically for the pure matter ($\Omega_{NR}=1$), pure radiation ($\Omega_R=1$), cosmological constant dominated ($\Lambda\neq 0$), string network, and curvature dominated ($k<0$) models. The resulting expressions are:

$$H_0 t = \frac{2}{3}(1+z)^{-3/2} \qquad (\Omega_{NR}=1), \tag{14a}$$

$$H_0 t = \frac{1}{2}(1+z)^{-2} \qquad (\Omega_R=1), \tag{14b}$$

$$H_0 t = \frac{2}{3\Omega_\Lambda^{1/2}} \left[\ln \left(\frac{\sqrt{\Omega_\Lambda (1+z)^{-3}} + \sqrt{\Omega_\Lambda (1+z)^{-3} + \Omega_{NR}}}{\sqrt{\Omega_{NR}}} \right) \right] \qquad (\Lambda \neq 0), \qquad (14c)$$

$$H_0 t = \left[(1-\Omega_{NR})^{-1} - \frac{\Omega_{NR}}{2} (1-\Omega_{NR})^{-3/2} \Psi(1+z) \right] \qquad (k<0 \ / \ NET), \qquad (14d)$$

where

$$\Psi(1+z) = \cosh^{-1} \left[\frac{2(1-\Omega_{NR})}{\Omega_{NR}} (1+z)^{-1} + 1 \right]. \qquad (14e)$$

Expression (13b) has been evaluated numerically for the decaying particle case (Turner 1985c), and for the fast-moving string case (Turner 1985b). Details for the fast-moving string dominated model are discussed in the Appendix.

The lookback time, $H_0(t_0 - t)$, is probably the most useful age related discriminator. A plot of lookback time vs. redshift, comparing all the models (with $\Omega_{NR}=0.25$ in those models with a smooth component) is shown in Figure 2. At a given redshift, the cosmological constant dominated model is the oldest; the radiation-dominated, the youngest. The use of Figure 2 in discriminating between models relies upon comparing a physical timescale to a redshift interval. Examples of physical timescales are the age of a galaxy at redshift $z=1$, or the theoretically determined time required for the change in color observed between two galaxies of the same type that can be identified at two different redshifts. The redshift interval can be expressed, for a given model, as a fraction of the total lookback time (the present age), with the use of Figure 2. The present age of the Universe can be obtained by dividing the timescale by the fraction of the total lookback time for the model being considered. If this age does not agree, within errors, with ages determined by independent means, such as the ages of globular clusters or nucleocosmochronology (Philip, Davis, and Hayes 1981; Sandage 1982; Schramm 1983; Iben 1984), the model can be ruled out.

B. Present age

The points at which the curves in Figure 2 cross the vertical axis on the right side of the plot give the present ages of the Universe for the various models. This age itself can also be used as a discriminator. The present age is simply $H_0 t(z=0)$, derived from equations (14a)-(14d). For the case of pure matter, equation (14a) yields the familiar result $H_0 t_0 = 2/3$, and for pure radiation the present age is given, by equation (14b), as $H_0 t_0 = 1/2$. Ages of the Universe for the various models with a smooth component are given in Table 1.

The large range of values in Table 1 implies that the age of the models is, in principle, a way of distinguishing between them. Radiation-dominated models tend to be very youthful ($H_0 t_0 = 0.5$–0.6), while $\Lambda \neq 0$ models tend to be rather old ($H_0 t_0 > 2/3$). Unfortunately, there is presently no definitive determination of $H_0 t_0$. H_0 is generally believed to be in the range 40–100 $km\ s^{-1} Mpc^{-1}$ = $(25\,Gyr)^{-1}$–$(10\,Gyr)^{-1}$ (Sandage and Tammann 1982; Aaronson and Mould 1983; Buta and deVaucouleurs 1983; Sandage and Tammann 1984; Arnett, Branch, Wheeler 1985; Huchra 1986; Sandage and Tammann 1986). The age of the Universe has been determined by a variety of methods including dating of globular clusters and nucleocosmochronology. These determinations suggest a value of t_0 in the range 12-18 Gyr (Philip, Davis, and Hayes 1981; Sandage 1982; Schramm 1983; Iben 1984). Taking these ranges for H_0 and t_0, $H_0 t_0$ is constrained only to the range: $0.48 \leq H_0 t_0 \leq 1.8$. If $H_0 t_0$ were shown to be ≥ 0.6 the decaying particle models would be ruled out. If $H_0 t_0$ were shown to be ≥ 1 only the $\Lambda \neq 0$ models would be viable. On the other hand, if H_0 were determined to be $50 km\ s^{-1} Mpc^{-1}$, then $H_0 t_0 \leq 0.72$ and a cosmological constant dominated model would be untenable.

C. Proper distance

The proper distance to an object of redshift z is needed to calculate the luminosity distance, angle distance, and proper volume of a comoving volume element in sections. The microwave temperature fluctuations induced by density perturbations on a given angular scale are also related to the proper distance of an object of redshift z.

The proper distance to an object of redshift z is the present value of the scale factor times the coordinate distance covered by a photon from redshift z until today:

$$d_0(z)=a(t_0)\int_{t(1+z)}^{t_0} dt'/a(t')=H_0^{-1}\int_{(1+z)^{-1}a_0}^{1} a_0\,da/\left[(H/H_0)a^2\right]. \tag{15}$$

The analytic solutions for the pure matter, pure radiation and curvature dominated (or string network) models are:

$$H_0 d_0(z)=2\left[1-(1+z)^{-1/2}\right] \qquad (\Omega_{NR}=1), \tag{16a}$$

$$H_0 d_0(z)=\frac{z}{1+z} \qquad (\Omega_R=1), \tag{16b}$$

$$H_0 d_0=\sqrt{\frac{1}{1-\Omega_{NR}}}\left[\Psi(1)-\Psi(1+z)\right] \qquad (k<0\ /\ NET), \tag{16c}$$

where $\Psi(1+z)$ is defined in (14e). For the other three models, the integral must be evaluated numerically.

The angular size of an object is inversely proportional to the proper distance, $H_0 d_0(z)$. For an object whose proper size scales with the expansion, $l(z)=l_0/(1+z)$, e.g., the wavelength of a given Fourier mode of the density fluctuations (in the linear regime), the angular size θ is given by

$$\theta=H_0 l_0/H_0 d_0(z). \tag{17}$$

The microwave temperature fluctuations on a given angular scale are related to the density contrast at last scattering, $z\simeq 1500$, on the length scale corresponding to this angle (see, e.g., Vittorio and Silk 1984 or Bond and Efstathiou 1984).

Values of $H_0 d_0(1500)$ for the six models are given in Table 2.

D. Luminosity distance

The luminosity distance to an object is defined as

$$d_L=\left[\frac{L}{4\pi l}\right]^{1/2}=r_1 a(t_0)(1+z) \tag{15}$$

where l is its apparent luminosity, L is its absolute luminosity, and r_1 is the coordinate distance to the object. For flat models, $d_0=a(t_0)r_1$, and thus the luminosity distance becomes

$$H_0 d_L=H_0 d_0(1+z). \tag{16}$$

For curvature-dominated models

$$H_0 d_L=\sqrt{\frac{1}{1-\Omega_{NR}}}\sinh\left[H_0 d_0\left(\frac{1}{1-\Omega_{NR}}\right)^{-1/2}\right](1+z) \qquad k<0. \tag{17}$$

From equations (16), (19), and (20) the following analytic expressions for the luminosity distance follow:

$$H_0 d_L=2\left[1-(1+z)^{-1/2}\right](1+z) \qquad (\Omega_{NR}=1), \tag{21a}$$

$$H_0 d_L=z \qquad (\Omega_R=1), \tag{21b}$$

$$H_0 d_L=\sqrt{\frac{1}{1-\Omega_{NR}}}\sinh\left[\Psi(1)-\Psi(1+z)\right](1+z) \qquad (k<0), \tag{21c}$$

$$H_0 d_L=\sqrt{\frac{1}{1-\Omega_{NR}}}\left[\Psi(1)-\Psi(1+z)\right](1+z) \qquad (NET). \tag{21d}$$

For all the other models, the proper distance and luminosity distance-redshift relationships must be calculated numerically. Figure 3 is a plot of the luminosity distance-redshift relationship, the classical Hubble diagram, for all models.

To date, much effort has been focused on the determination of q_0 which appears in the power series expansion for d_L:

$$H_0 d_L=z+\frac{1}{2}(1-q_0)z^2+\cdots \tag{22}$$

In order to use this diagram to distinguish between models, it is necessary to have a sample of objects with known absolute magnitudes (standard candles) out

to reasonably high redshifts. Often the first-ranked galaxies in clusters are used as standard candles. The observed magnitude must be corrected for many effects which are not well determined, such as evolution and statistical selection effects. At present, the errors in the corrections are of a magnitude such that distinguishing between models, with this diagram, is not possible.

E. Angle distance

The angle distance, d_A, is the ratio of the diameter of the source, D (assumed here to be independent of redshift), to its angular diameter $\theta = D/a(t_1)r_1$:

$$d_A = a(t_1)r_1 = a(t_0)r_1(1+z)^{-1}. \tag{23}$$

In terms of the proper distance this becomes

$$H_0 d_A = H_0 d_0 (1+z)^{-1} \qquad (k=0), \tag{24a}$$

$$H_0 d_A = \sqrt{\frac{1}{1-\Omega_{NR}}}\sinh\left[H_0 d_0\left(\frac{1}{1-\Omega_{NR}}\right)^{-1/2}\right](1+z)^{-1} \qquad (k<0). \tag{24b}$$

Comparing (18) and (23), we see that the angle distance and the luminosity distance are not independent cosmological probes. For example, when the quantities l and θ are combined to obtain the surface brightness, $l/\theta^2 \sim (1+z)^{-4}$, all dependences on the cosmological model cancel. Thus the surface brightness, in principle, provides a means of isolating evolutionary effects. This could be very important, since, in an observational angle distance diagram, evolutionary and cosmological effects are intermixed.

The expressions for angle distance in the simplest models follow from equation (24):

$$H_0 d_A = 2\left[1-(1+z)^{-1/2}\right](1+z)^{-1} \qquad (\Omega_{NR}=1), \tag{25a}$$

$$H_0 d_A = \frac{z}{(1+z)^2} \qquad (\Omega_R=1), \tag{25b}$$

$$H_0 d_A = \sqrt{\frac{1}{1-\Omega_{NR}}}\sinh\left[\Psi(1)-\Psi(1+z)\right](1+z)^{-1} \qquad (k<0), \tag{25c}$$

$$H_0 d_A = \sqrt{\frac{1}{1-\Omega_{NR}}}\left[\Psi(1)-\Psi(1+z)\right](1+z)^{-1} \qquad (NET). \qquad (25d)$$

The theoretical angle distance vs. redshift curves are shown in Figure 4. At low redshifts, the angular diameter ($\sim 1/d_A$) of an object decreases with increasing redshift, as expected. It reaches a minimum at a redshift $z=2$ then rises with increasing redshift. The increase in angular diameter with redshift can be understood because the light we observe today from an object at higher redshift was emitted when the object was closer to us.

With the recent advent of the use of two-dimensional digital devices, it has become possible to measure angular diameters for many galaxies. When doing so, It is essential to define the angular diameter in terms of metric rather than isophotal size. The metric size is defined in terms of a physical part of the galaxy image that can be conveniently identified in a plot of some physical quantity vs. θ. An example of such a quantity is the radius (or angle θ) at which the quantity $d \ln L(r)/d \ln r$ has some chosen value. (For further discussion, see, Djorgovski and Spinrad 1981 or Crawford 1981).

The divergence of the angle distance-redshift curves at large redshifts suggests that having a higher redshift sample would allow great cosmological leverage. Unfortunately, since objects at higher redshifts are fainter, measurements have lower precision, and therefore objects at higher redshifts do not necessarily provide better cosmological leverage. Kron (1985) estimates that the peak of the cosmological leverage vs. redshift curve occurs for $z \simeq 0.4$ for a measurement of a quantity that combines counts and angle distance.

F. Comoving volume element

The number of galaxies in a volume element, $dzd\Omega$, is just the number density of galaxies (per comoving volume) times the comoving volume, dV_0, of that volume element. In flat models, the comoving volume dV_0 (which for simplicity

we take to be equal to the proper volume today) is just

$$dV_0=\frac{d}{dz}\left(d_0(z)^3/3\right)\,dzd\Omega=H^{-1}(z)\,d_0^2(z)\,dzd\Omega \tag{26}$$

In models with a curvature term,

$$dV_0=H^{-1}(z)\,d_L^2(z)(1+z)^{-2}dzd\Omega. \tag{27}$$

In the absence of evolution the number of galaxies per comoving volume element is independent of the redshift, z, and therefore the number of galaxies in $dzd\Omega$ is simply proportional to $dV_0/dzd\Omega$. Analytic expressions for the comoving volume element follow from equation (16) and the Friedmann equation:

$$\frac{dV_0}{dzd\Omega}=4\left[(1+z)^{-3/4}-(1+z)^{-5/4}\right]^2H_0^{-3} \qquad (\Omega_{NR}=1), \tag{28a}$$

$$\frac{dV_0}{dzd\Omega}=\frac{z^2}{(1+z)^4}H_0^{-3} \qquad (\Omega_R=1), \tag{28b}$$

$$\frac{dV_0}{dzd\Omega}=\frac{1}{1-\Omega_{NR}}\sinh^2\left[\Psi(1)-\Psi(1+z)\right] \times\left[\Omega_{NR}(1+z)^3+(1-\Omega_{NR})(1+z)^2\right]^{-1/2}H_0^{-3} \qquad (k<0) \tag{28c}$$

$$\frac{dV_0}{dzd\Omega}=\frac{1}{1-\Omega_{NR}}\left[\Psi(1)-\Psi(1+z)\right]^2 \times\left[\Omega_{NR}(1+z)^3+(1-\Omega_{NR})(1+z)^2\right]^{-1/2}H_0^{-3} \qquad (NET). \tag{28d}$$

For the $\Lambda\neq 0$, fast-moving string, and decaying particle models, $dV_0/dzd\Omega$ must be obtained numerically.

$dV_0/dzd\Omega$ is shown in Figure 5. From this plot we see that in a given redshift interval we would count the most galaxies for a cosmological constant dominated model and the least for a radiation-dominated model. Unfortunately faint galaxy surveys are magnitude, rather than redshift, limited samples. Models with a larger comoving volume element also have a smaller luminosity distance. These two effects nearly balance, so that counts in a magnitude limited sample are not as useful in distinguishing between models as Figure 5 seems to suggest. Counts in a redshift limited sample, however, could be put to good use in distinguishing between the various flat models.

Recently, Loh and Spillar (1986a,b) have attempted such a count-redshift test, by determining redshifts and fluxes of 1000 field galaxies. Their three data points (at z=0.25, 0.5, 0.75) are displayed on our Figure 5. Loh (1986) interprets these results to constrain $0.8 \leq \Omega_{NR} \leq 1.5$ and $-0.5 \leq \Omega_\Lambda \leq 0.2$. We see that the Loh and Spillar data points could only marginally allow flat FS or β^{-1}=10 decaying particle models. The other flat models, with Ω_{NR}=0.25, are not compatible with the data points. These results are indicative of the significant cosmological leverage that is provided by a comoving volume-redshift test.

F. Growth of density fluctuations

A final kinematical consideration is the growth of the density fluctuations which lead to the structure observed in the Universe. The smaller the growth since decoupling (when all the models considered are dominated by the NR component) the larger the initial perturbations required at decoupling. Measurements of the smoothness of the cosmic background radiation can be used to place an upper limit on the size of density perturbations at decoupling, and thus a lower limit to growth since decoupling (Bond and Efstathiou 1984; Vittorio and Silk 1984; Turner 1985a; Vittorio and Silk 1985; Kolb, Olive, and Vittorio 1986).

The growth of linear density perturbations in component i, $\delta_i = \delta\rho_i/\rho_i$, of a multi-component fluid, is governed by the equation

$$\ddot{\delta}_i + \frac{2\dot{a}}{a}\dot{\delta}_i + \left(\frac{v_{si}^2 q^2}{a^2} - 4\pi G\rho \sum_i \frac{\rho_i}{\rho} \right) \delta_i = 0, \qquad (29)$$

where $q = 2\pi a/\lambda$ is the comoving wavenumber of the perturbation and $v_{si} = (dp_i/d\rho_i)^{1/2}$ is the sound speed in component i. (See Peebles 1980 for a more complete discussion of equation (29).) The pressure term, $v_{si}^2 q^2/a^2$, can be neglected when the wavenumber, q, is much less than the Jeans wavenumber. With the assumption that the smooth component does not clump, so that δ_{SM} is

always 0, equation (29) takes the following form for the non-relativistic component (for $q \ll q_j$):

$$\ddot{\delta}_{NR}+2H\dot{\delta}_{NR}-\frac{3}{2}H^2\Omega_{NR}\delta_{NR}=0. \tag{30}$$

When considering the case of pure matter, $\Omega_{NR}=1$, equation (30) yields the familiar result that $\delta_{NR} \propto t^{2/3}$, or $\delta_{NR} \propto a$. The growth of perturbations since decoupling in such a model is just $1+z_{dec} \simeq 1500$.

In the case that $\Omega_R \gg \Omega_{NR}$, density perturbations in the NR component do not grow (unless they had some initial velocity $\dot{\delta}_{NR}$ in which case $\delta_{NR} \propto \ln a$). For $\Lambda \neq 0$, the decaying particle, and the string-dominated models, we have solved equation (30) numerically. The solution for fast-moving string dominated models is discussed in more detail in the Appendix. An analytic solution is possible for $k<0$ (or string network) models. The growth of δ_{NR} since a redshift z is given by

$$\frac{5(1+z)}{(\cosh\Psi_0-1)^3}[-3\Psi_0\sinh\Psi_0+(\cosh\Psi_0-1)(\cosh\Psi_0+5)]. \tag{31}$$

where Ψ is evaluated at the present ($z=0$).

The evolution of δ_{NR} since decoupling (when all the models were dominated by the NR component) is shown in Figure 6, and the total growth since decoupling for $\Omega_{NR}=0.25$ is displayed in Figure 7. The cases of decaying particles and light strings are discussed in more detail by Turner (1985b,c). Fry (1985) has also considered the growth of density perturbations in some of the smooth component models discussed here.

IV. Summary

As we have seen, the evolution of the cosmic scale factor $a(t)$ in these exotic flat models with a smooth component is very different from that in an $\Omega=1$ matter-dominated model, which in turn means that the kinematics of these models are quite different. The largest deviations from the canonical matter-

dominated Einstein-deSitter models occurs in the $\Lambda \neq 0$ and decaying particle models.

Linear density perturbations grow more slowly (as a function of $a(t)$) in the smooth component models than in a matter-dominated flat model. In this regard, the $\Lambda \neq 0$ model comes closest to the matter-dominated model and the growth of perturbations is most inhibited in the model with fast-moving strings. Slower growth of density perturbations means that larger perturbations are required early on (say at decoupling) in order to achieve the same degree of inhomogeneity today. Larger density perturbations at decoupling imply larger predicted anisotropies in the microwave background, which places severe restrictions on the models.

The most powerful discriminator may be the present age of the model. The dimensionless ratio $H_0 t_0$ varies from around 0.55 for the decaying particle models, to 2/3 for the canonical flat model, to greater than unity for some of the $\Lambda \neq 0$ models. A value of $H_0 t_0 \geq 0.6$ essentially rules out decaying particle models, while a value of $H_0 t_0 \geq 1.0$ forces us to models with $\Lambda \neq 0$. The lookback time vs. redshift also appears to be a very promising test.

We will conclude by contrasting the present situation to that 25 years ago. A quarter of a century ago Sandage (1961), in his paper "The Ability of the 200-inch Telescope To Discriminate Between Selected World Models", reviewed many of the tests discussed here. Although in the intervening years a large amount of effort has been devoted to cosmological tests, our conclusions are not qualitatively dissimilar to his.

Sandage (1961) chose to review only models where $\Lambda \neq 0$ since "the large variety of possible world models makes a final decision between the models impossible because there are more parameters in the equations than can be determined observationally". Today, with the numerous smooth component

candidates, this problem is accentuated. In addition, we can also have a range of values for Ω_{NR}, which leads to overlap of the curves for the various flat models.

Sandage (1961) concluded that "it appears possible to find q_0 from the magnitude-redshift relation", and cites $q_0=1\pm1/2$ as a most probable value. Most recent efforts have focused on this approach, but unfortunately q_0 has not been unambiguously determined. We see, in Figure 3, that the differences between the various flat models are small, and since the uncertainties in corrections are of a magnitude comparable to these differences, it seems that alternative approaches should also be considered.

One such approach (Loh and Spillar 1986a,b; Loh 1986) is the comoving volume element vs. redshift test. Sandage (1961), with only magnitude limited counts available, was forced to conclude that "the predicted differences between the models are too small compared with the known fluctuations of the distribution." Redshift samples that are now accessible (Koo 1985; Loh and Spillar 1986a) provide much more cosmological leverage. In fact, in Figure 5, the differences between the $\Lambda\neq0$ model and the decaying particle models can be quite substantial at redshifts of order a few.

With the realization of the importance of defining angular diameters in terms of their metric size, Sandage (1961) concluded that "a test for q_0 seems to be possible with the 200-inch, and the test will be difficult and perhaps marginal". Today, we draw basically the same conclusion, although with the use of two-dimensional digital devices, perhaps we can be somewhat more optimistic.

Finally, Sandage (1961) concluded that "a decision between the possible classes of models cannot be made until observations are pushed near to, or perhaps beyond, the telescopic limit of the 200-inch". In 1986, our models and "telescopic limits" are different, but our conclusion is much the same: With the advent of generation of space-based observatories such as the Hubble Space

Telescope and SIRTF, and larger, better-instrumented ground-based facilities it may be possible to discriminate between the different flat models.

Acknowledgements

We are grateful to Richard Kron for many enlightening conversations. This work was supported in part by the DOE (at Chicago and Fermilab), the NASA (at Fermilab), and the NSF (at Chicago). MST receives support from an Alfred P. Sloan Fellowship.

Appendix

Here we consider the flat (k=0) model with Ω_{NR}=0.1–0.3 where the smooth component is in fast-moving strings. This possibility was suggested by Vilenkin (1984). The crucial aspect of these strings is the fact that their mass density of strings scales as

$$\rho_{FS} \propto \frac{1}{a(t)\ t} \tag{A1}$$

Here we will solve for the evolution of the scale factor $a(t)$, the growth of density fluctuations, and the proper distance.

The density of the two components, non-relativistic particles (NR) and light, fast-moving strings (FS), evolve as

$$\rho_{NR}=\rho_{NRi}\left(\frac{a}{a_i}\right)^{-3}, \tag{A2a}$$

$$\rho_{FS}=\rho_{FSi}\left(\frac{a}{a_i}\right)^{-1}\left(\frac{t}{t_i}\right)^{-1}. \tag{A2b}$$

where subscript 'i' denotes some unspecifies initial epoch, which we take to be sufficiently early so that $\rho_{NR}>>\rho_{FS}$. The Friedmann equation takes the form

$$H^2=\left(\frac{\dot{a}}{a}\right)^2=\frac{8\pi G}{3}(\rho_{FS}+\rho_{NR}). \tag{A3}$$

With the following definitions:

$$x\equiv\frac{t}{t_i},$$

$$b\equiv\frac{\rho_{FS}}{\rho_{NR}}=b_i\,(a/a_i)^2/x,$$

$$a'\equiv\frac{da}{dx},$$

the Friedmann equation can be written as

$$\left(\frac{a'}{a}\right)^2=\frac{4}{9}\left[\left(\frac{a}{a_i}\right)^{-3}+b_i\left(\frac{a}{a_i}\right)^{-1}x^{-1}\right]. \tag{A4}$$

where we have used the fact that

$$H_i=\frac{8\pi G\rho_{NR}}{3}=\frac{2}{3}t_i^{-1}.$$

Beginning at $x_i=1$ and normalizing $a(t)$ so that $a_i=a(t_i)=1$, equation (A4) becomes

$$\left(\frac{a'}{a}\right)^2=\frac{4}{9}\left[a^{-3}+b_i a^{-1}x^{-1}\right]. \tag{A5}$$

For our numerical calculation we choose the initial epoch such that

$$b_i=\frac{\rho_{FSi}}{\rho_{NRi}}=0.01<<1. \tag{A6}$$

Early on, the second term on the right hand side of equation (A5) is small and $a\,\alpha\,x^{2/3}$ as expected in a matter-dominated model. When $b>>1$, $a\alpha t$ and $\rho_{FS}\alpha\, a^{-2}$ as in a curvature-dominated model.

Although we are interested in a variety of values for Ω_{NR}, equation (A5) need only be solved once. Beginning with the arbitrary initial conditions, $x_i=1$ and $a_i=1$, the present epoch is identified by finding the time at which the value of b corresponds to its value ($b_0\equiv\Omega_{FS}/\Omega_{NR}=(1-\Omega_{NR})/\Omega_{NR}$) today.

Equation (25), which gives the growth of density perturbations in the NR component, now takes the form

$$\delta_{NR}''+2H\delta_{NR}'-\left[\frac{3}{2}\left(\frac{a'}{a}\right)^2\left(1+0.01a^2x^{-1}\right)^{-1}\right]\delta_{NR}=0. \tag{A7}$$

Equation (A7) is solved simultaneously with equation (A5) to determine the growth of density fluctuations. Early on, the model is strongly matter-dominated, $a\,\alpha\,x^{2/3}$, and $\rho_{FS}\,\alpha\,x^{-2.5}$. As expected, the growing mode of density fluctuations evolves as $\delta\,\alpha\,x^{2/3}$. When the model becomes string-dominated, $a\,\alpha\,x$, $\rho_{FS}\,\alpha\,x^{-2}$, and perturbations cease growing. The evolution of δ_{NR} is shown in Figure 6, and the growth of a perturbation since decoupling is shown in Figure 7.

The proper distance $d_0(z)$ is needed to calculate the various kinematic quan-

tities such as the luminosity distance, the angle distance, and the comoving volume element. It is obtained in a straightforward way by integrating equation (12).

Table 1 - The value of $H_0 t_0$

Ω_{NR}	decaying particles $\beta^{-1}=30$	$\Lambda \neq 0$	FS	$k < 0$	$\Omega_{NR}=1$	$\Omega_R=1$
				NET		
0.1	0.540	1.28	0.842	0.898		
0.15	0.525	1.16	0.816	0.870		
0.2	0.524	1.08	0.796	0.846	0.667	0.5
0.25	0.526	1.01	0.779	0.826		
0.3	0.530	0.96	0.765	0.809		

Table 2 - Proper distance to the last scattering surface $H_0 d_0(1500)$

Ω_{NR}	decaying particles $\beta^{-1}=30$	$\Lambda \neq 0$	FS	$k < 0$ NET	$\Omega_{NR}=1$	$\Omega_R=1$
0.1	1.24	4.95	3.28	2.32		
0.15	1.17	4.23	3.02	2.59		
0.2	1.15	3.78	2.84	2.78	1.95	1.00
0.25	1.14	3.46	2.70	2.94		
0.3	1.15	3.21	2.60	3.07		

References

Aaronson, M. and Mould, J. 1983, *Ap. J.*, **265**, 1.

Albrecht, A. and Steinhardt, P. 1982, *Phys. Rev. Lett.*, **48**, 1220.

Arnett, W. D., Branch, D., Wheeler, J. 1985, *Nature*, **314**, 337.

Audouze, J. and Tran Thanh Van, J., eds. 1983, *Formation and Evolution of Galaxies*, (Dordrecht: Reidel).

Bardeen, J. M., Bond, J., Kaiser, N., and Szalay, A. 1986, preprint.

Bond, J. and Efstathiou, G. 1984, *Ap. J. Lett.*, **285**, L44.

Bosma, A. 1981a, *A. J.*, **86**, 1791.

Bosma, A. 1981b, *A. J.*, **86**, 1825.

Buta, R. and deVaucouleurs, G. 1983, *Ap. J.*, **266**, 1.

Crawford, M. 1981, in *Neutrino 81*, eds. R. J. Cence, E. Ma, and A. Roberts (Honolulu: University of Hawaii).

Davis, M. and Peebles, P. J. E. 1983, *Ann. Rev. Astr. Ap.*, **21**, 109.

Dicke, R. H. and Peebles, P. J. E. 1979, in *General Relativity: An Einstein Centenary Survey*, eds. S. W. Hawking and W. Israel, (Cambridge: Cambridge Univ. Press).

Dicus, D. A., Kolb, E. W., and Teplitz, V. L. 1977, *Phys. Rev. Lett.*, **39**, 168.

Djorgovski, S. and Spinrad, H. 1981, *Ap. J.*, **251**, 417.

Faber, S. and Gallagher, J. 1979, *Ann. Rev. Astr. Ap.*, **17**, 135.

Fry, J. 1985, *Phys. Lett. B*, **158B**, 211.

Gelmini, G., Schramm, D. N., and Vallee, J. P. 1984, *Phys. Lett. B*, **99**, 411.

Gunn, J. E., and Oke, J. B. 1975, *Ap. J.*, **195**, 255.

Guth, A. 1981, *Phys. Rev. D*, **23**, 347.

Huchra, J. 1986, in *Inner Space/Outer Space Conf.*, eds. E. Kolb etal., (Chicago, University of Chicago Press).

Iben, I. 1984, *Phys. Rep.*, **105**, 329.

Kaiser, N. 1983, *Ap. J. Lett.*, **273**, L17.

Kaiser, N. 1985, *Ap. J. Lett.*, **284**, L9.

Kolb, E. W., Olive, K., and Vittorio, N. 1986, *Phys. Rev. D.*, submitted.

Koo, D. C. 1985, *Astr. J.*, **90**, 418.

Kormendy, J. and Knapp, J., eds. 1986, *IAU Symposium 117, Dark Matter in the Universe*, (Dordrecht: Reidel).

Kristian, J., Sandage, A., and Westphal, J. A. 1978, *Ap. J.*, **221**, 383.

Kron, R. 1985, lecture notes on Determination of Cosmological Parameters.

Linde, A. 1982, *Phys. Lett. B*, **108**, 289.

Loh, E. D. 1986, *Phys. Rev. Lett.*, submitted.

Loh, E. D. and Spillar, E. J. 1986a, *Ap. J.*, submitted.

Loh, E. D. and Spillar, E. J. 1986b, *Ap. J. Lett.*, submitted.

Olive, K., Seckel, D., and Vishniac, E. T. 1985, *Ap. J.*, **292**, 1.

Peebles, P. J. E. 1980, *The Large-Scale Structure of the Universe* (Princeton: Princeton University Press).

Peebles, P. J. E. 1984, *Ap. J.*, **284**, 439.

Philip, A. G., Davis, M., and Hayes, D. S., eds. 1981, *IAU Symposium 68, Astrophysical Parameters for Globular Clusters* (Schenectady, NY: L. Davis Press).

Press, W. and Davis, M. 1982, *Ap. J.*, **259**, 449.

Rubin, V. C., Ford, W. K., and Thonnard, N. 1978, *Ap. J. Lett.*, **225**, L107.

Rubin, V. C., Ford, W. K., and Thonnard, N. 1980, *Ap. J.*, **261**, 439.

Rubin, V. C. 1983, *Science*, **220**, 1339.

Sandage, A. 1961, *Ap. J.*, **133**, 355.

Sandage, A. 1982, *Ap. J.*, **252**, 553.

Sandage, A. and Tammann, G. A. 1982, *Ap. J.*, **256**, 339.

Sandage, A. and Tammann, G. A. 1984, *Nature*, **307**, 326.

Sandage, A. and Tammann, G. A. 1986, in *Inner Space/Outer Space,* eds. E. Kolb etal., (Chicago: University of Chicago Press).

Schramm, D. N. 1983, in *Highlights of Astronomy as Presented to the 18th General Assembly of the IAU,* Vol. 6, ed. R. West, (Dordrecht: Reidel).

Turner, M. S. 1985a, *Phys. Rev. Lett.*, **55**, 549.

Turner, M. S. 1985b, *Phys. Rev. Lett.*, **54**, 252.

Turner, M. S. 1985c, *Phys. Rev. D,* **31**, 1212.

Turner, M. S. 1986, in *IAU Symposium 117, Dark Matter in the Universe,* eds. J. Kormendy and J. Knapp (Dordrecht: Reidel).

Turner, M. S., Steigman, G., and Krauss, L. 1984, *Phys. Rev. Lett.*, **52**, 2090.

Vilenkin, A. 1984, *Phys. Rev. Lett.*, **53**, 1016.

Vilenkin, A. 1985, *Phys. Rep.*, **121**, 263.

Vittorio, N. and Silk, J. 1984, *Ap. J. Lett.*, **285**, L39.

Vittorio, N. and Silk, J. 1985, *Phys. Rev. Lett.*, **54**, 2269.

Vittorio, N. and Turner, M. S. 1986, *Ap. J.*, submitted.

Weinberg, S. 1972, *Gravitation and Cosmology* (New York: John Wiley and Sons).

Yang, J., Turner, M. S., Steigman, G., Schramm, D. N., and Olive, K. 1984, *Ap. J.*, **281**, 493.

Figure Captions

Figure 1:

The evolution of the scale factor $a(t)$ for the various models (with Ω_{NR}=0.25 in those models with a smooth component). "30" denotes the decaying particle model with β^{-1}=30; R, Ω_R=1; FS, light, fast-moving, non-intercommuting strings; and NET, a network of light strings. The bold line represents the model with Ω_{NR}=1.

Figure 2:

The lookback time-redshift relationship. The bold line represents the model with Ω_{NR}=1. "30" and "10" are values of β^{-1} in decaying particles models. Labels are the same as in Figure 1, and Ω_{NR}=0.25. In general the ordering of the curves is determined by the relative pressure in the smooth component, γ_{SM}, going from negative pressure ($\Lambda \neq 0$) to zero pressure (Ω_{NR}=1) to positive pressure (Ω_R=1).

Figure 3:

Luminosity distance-redshift relationship. Ω_{NR}=0.25, and labels are the same as in Figure 2.

Figure 4:

Angle distance-redshift relationship. Ω_{NR}=0.25, and labels are the same as in Figure 2.

Figure 5:

Comoving volume element-redshift relationship. Ω_{NR}=0.25 and labels are the same as in Figure 2. The points with error bars are the Loh and Spillar (1986b) data points.

Figure 6:

Evolution of δ_{NR} since decoupling. The various symbols mark the values of a/a_0 for which Ω_{NR} has the indicated values. Labels are the same as in Figure 2.

Figure 7:

Total growth of linear density perturbations since decoupling for Ω_{NR}=0.25. Labels are the same as in Figure 2, with the addition that "100" refers to a decaying particle model with β^{-1}=100.

Figure 1

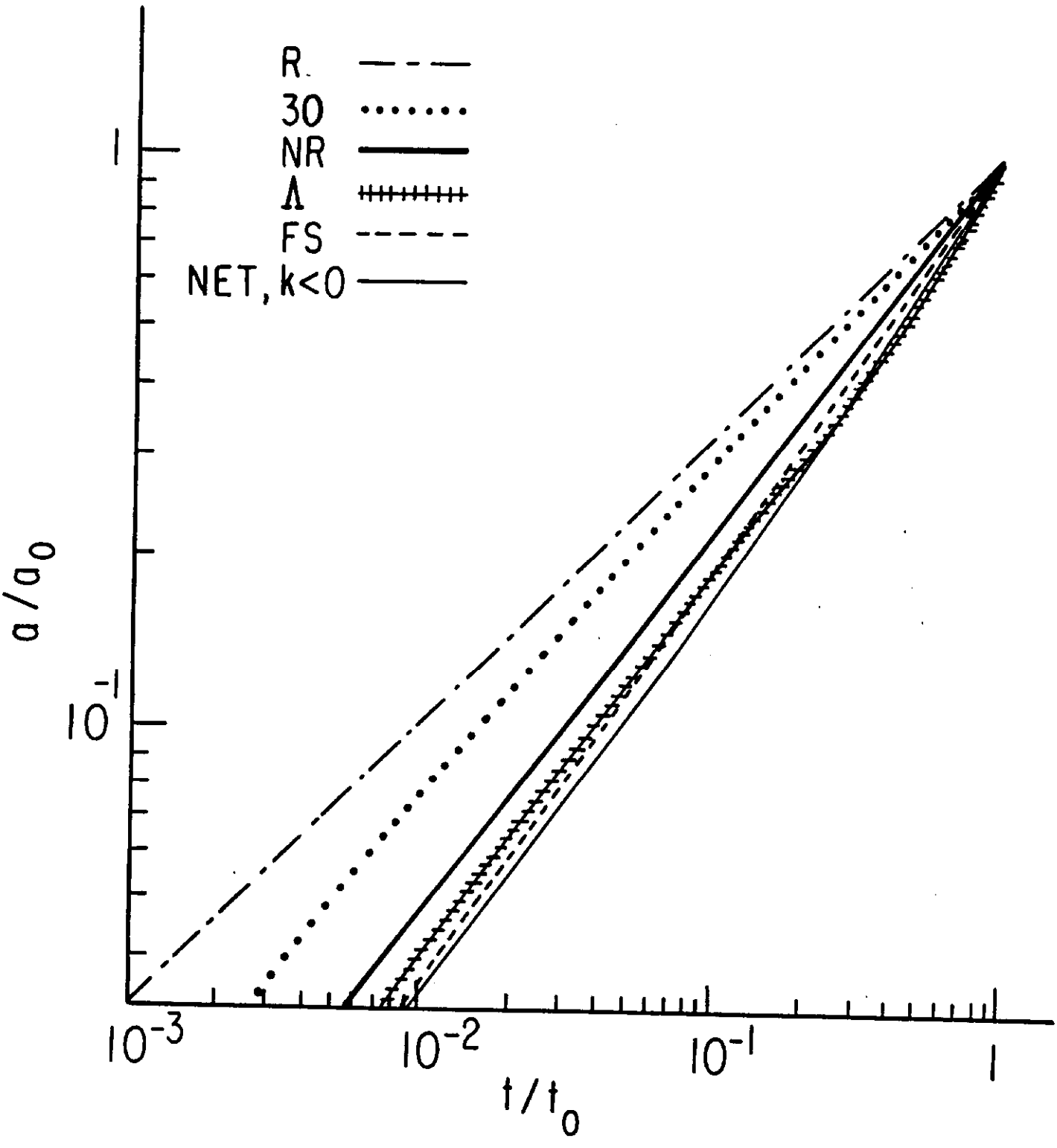

Figure 2

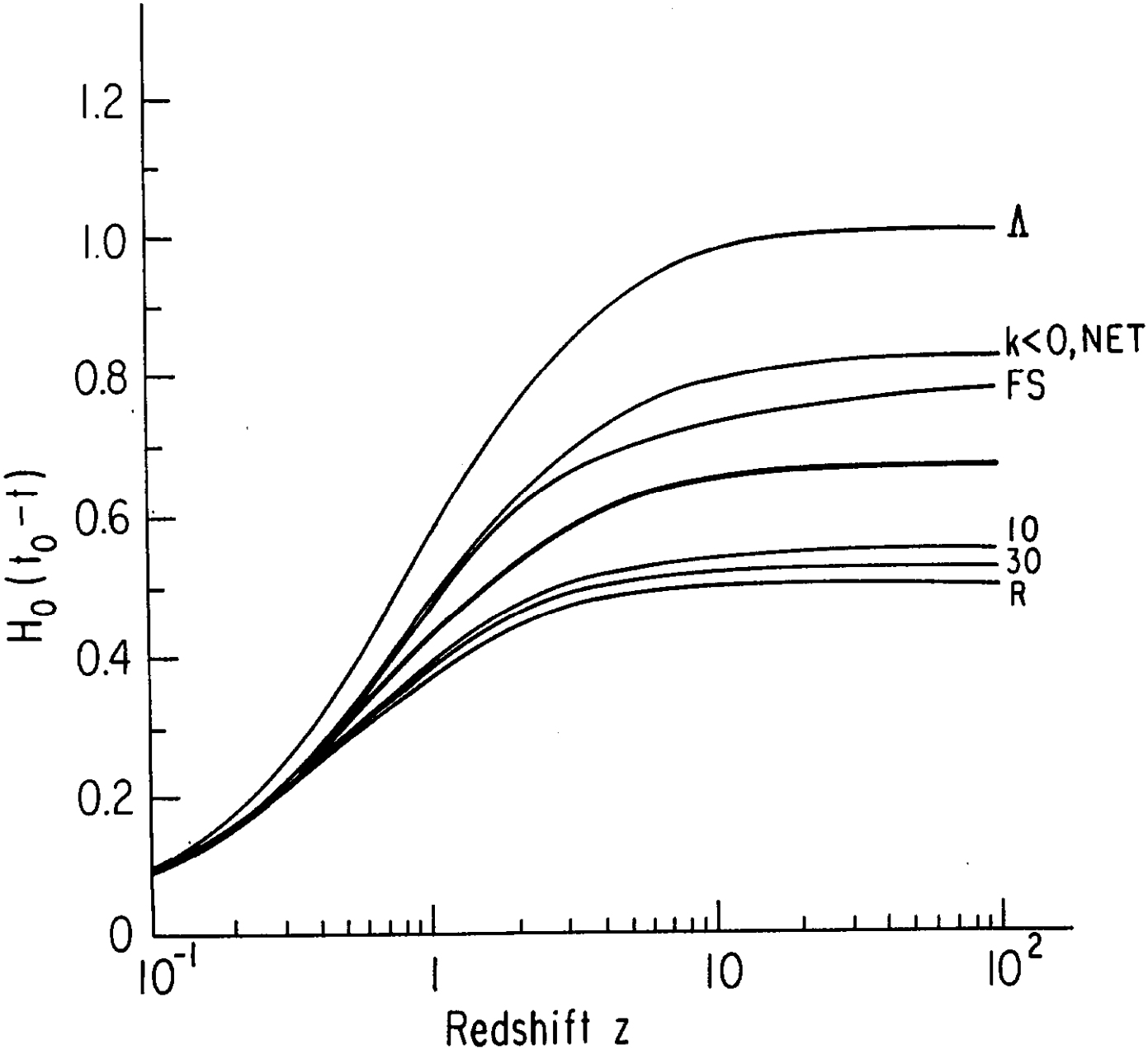

Figure 3

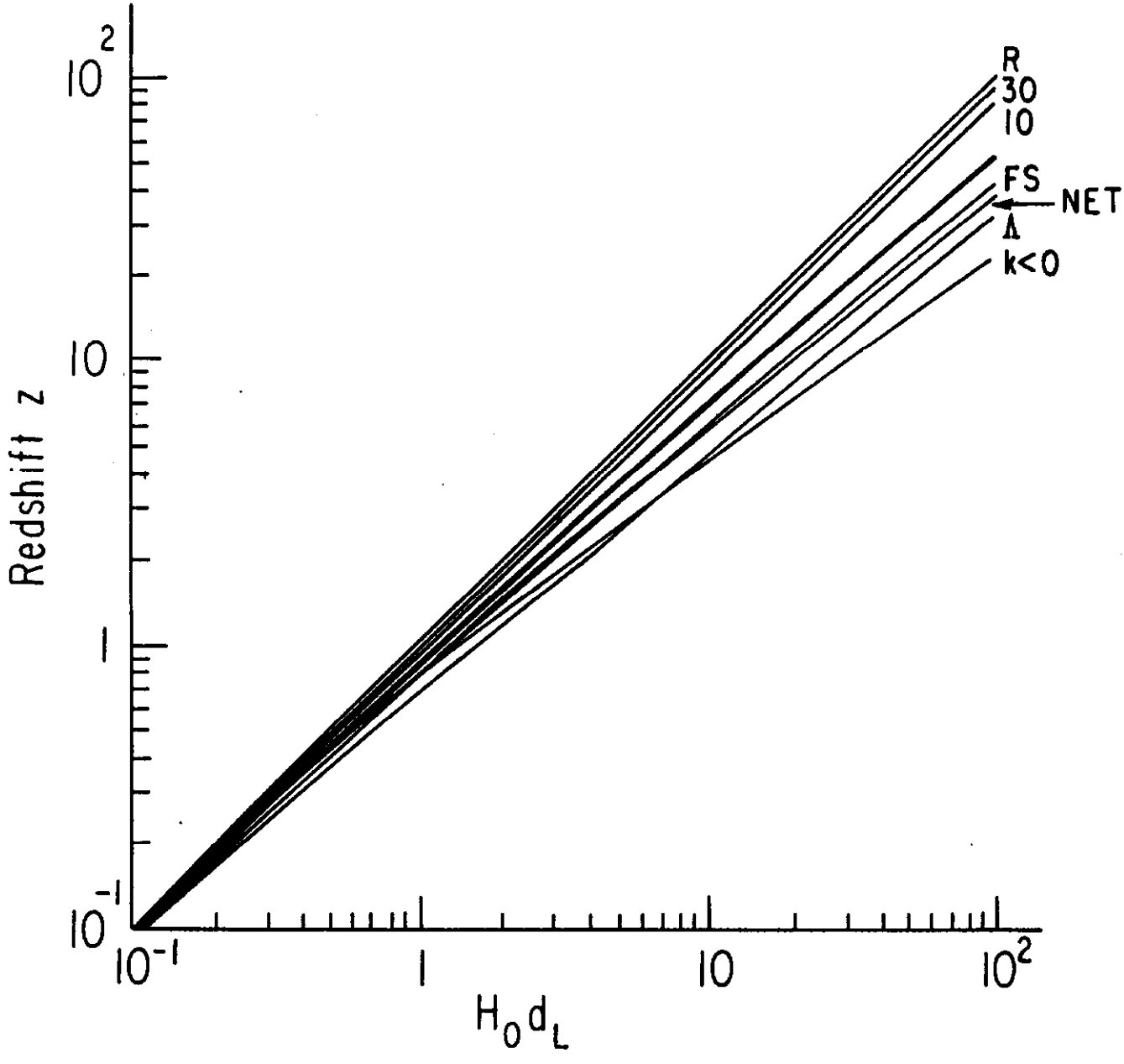

Figure 4

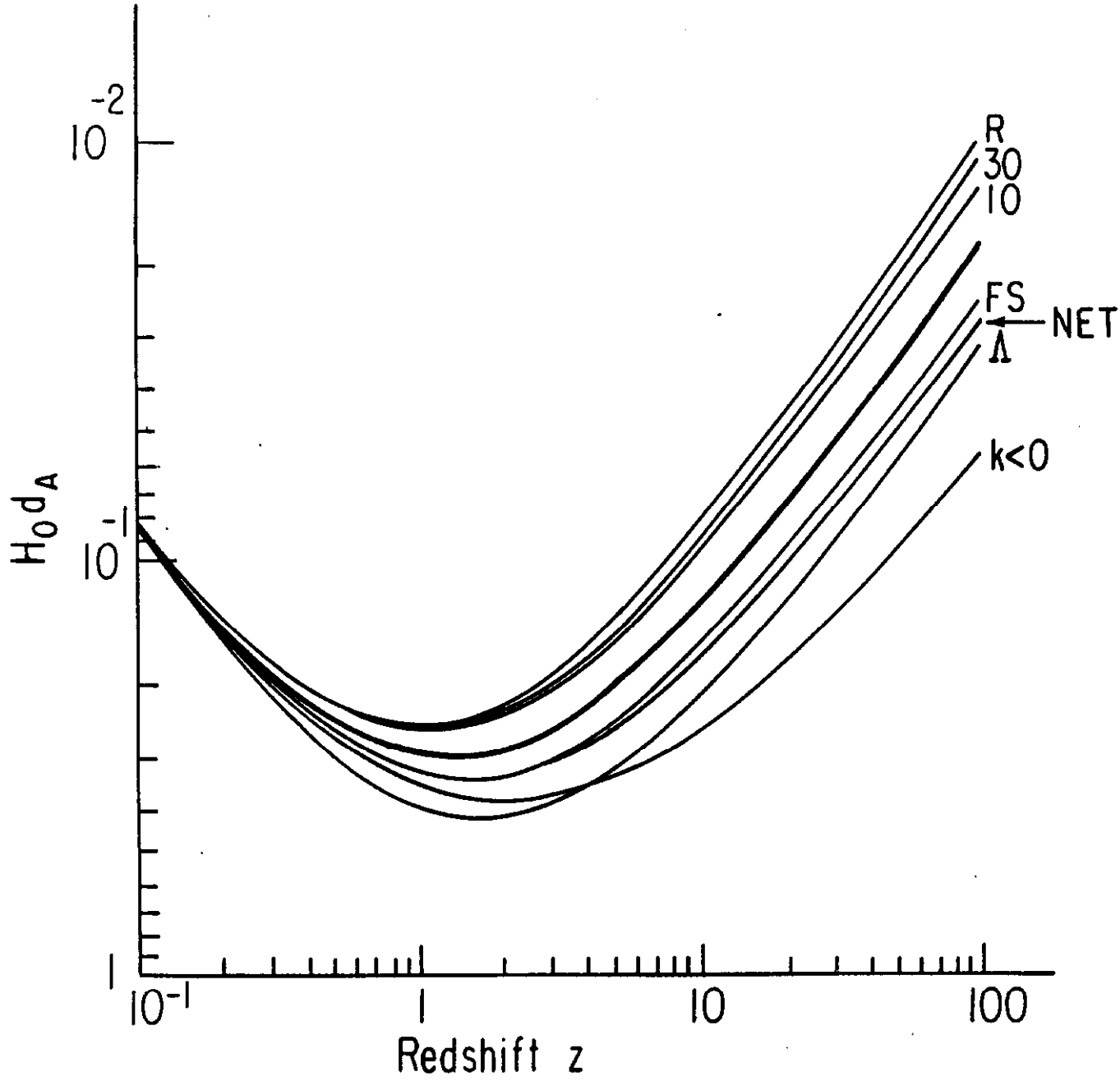

Figure 5

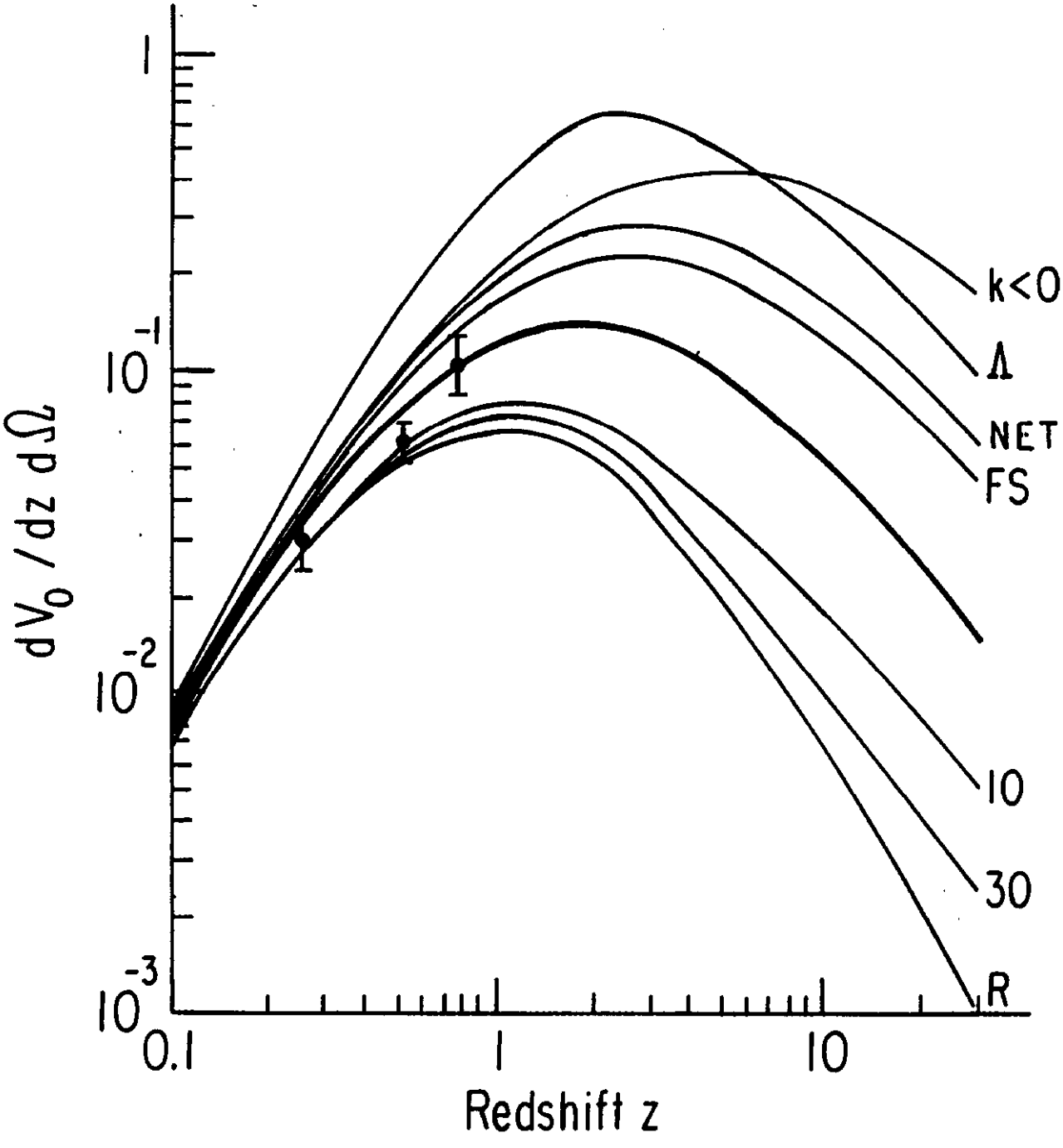

Figure 6

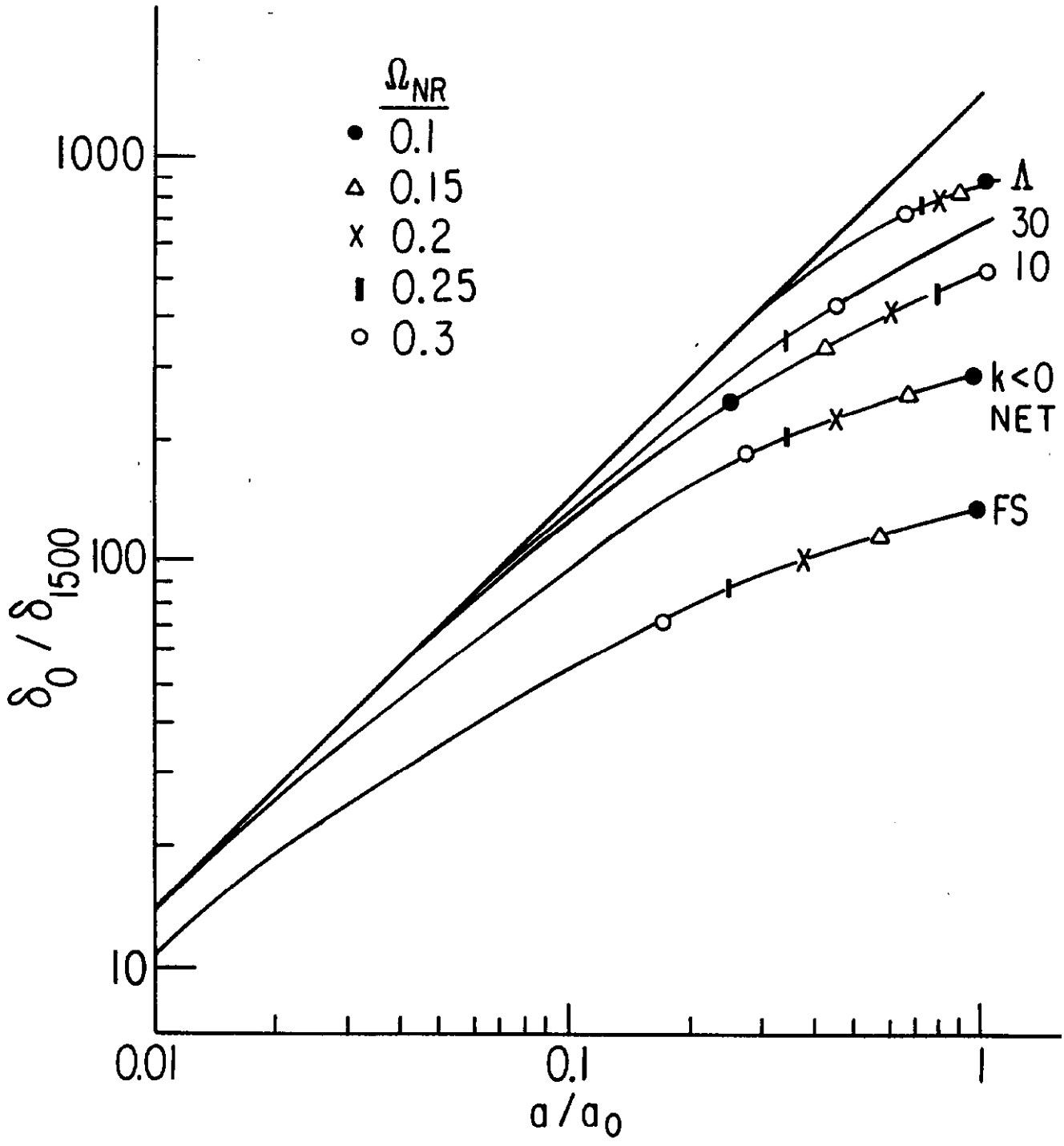
Ω_{NR}
0.1
0.15
0.2
0.25
0.3
1000
100
10
δ_0 / δ_{1500}
0.01
0.1
1
a/a_0
Λ
30
10
k<0
NET
FS

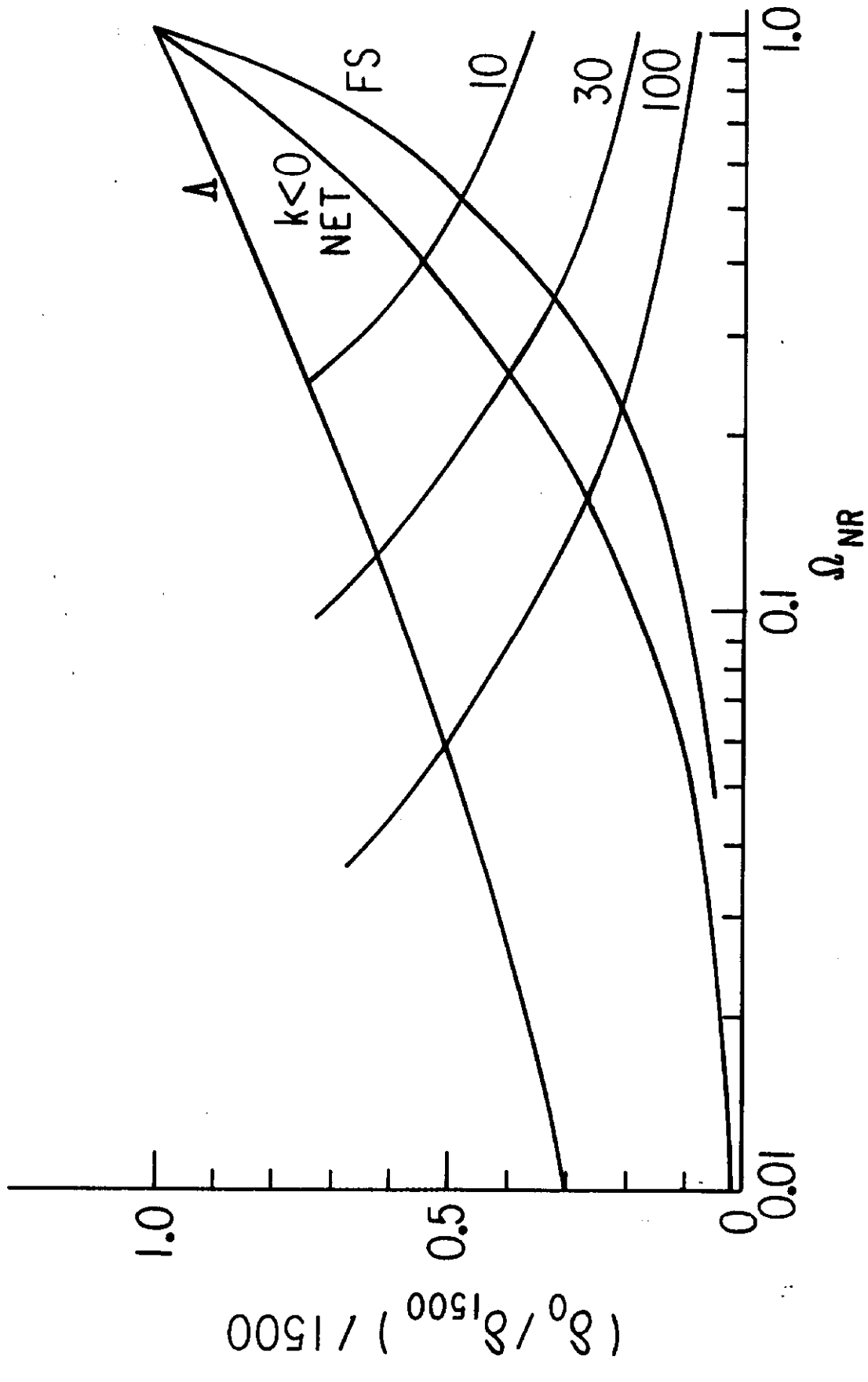
$(\delta_0/\delta_{1500})/1500$
1.0
0.5
0
0.01
0.1
1.0
Ω_{NR}
Λ
k<0
NET
FS
10
30
100

Figure 7